# X-Ray Diffraction from a Dense Plasma

D. Riley,[1] N. C. Woolsey,[1,*] D. McSherry,[1] I. Weaver,[1] A. Djaoui,[2] and E. Nardi[3]
[1]*School of Mathematics and Physics, Queens University of Belfast, Belfast BT7 1NN, United Kingdom*
[2]*Rutherford-Appleton Laboratory, Chilton, Didcot OX11 OQX, United Kingdom*
[3]*Department of Particle Physics, Weizmann Institute of Science, Il-76100 Rehovot, Israel*
(Received 9 February 1999; revised manuscript received 22 October 1999)

We report measurements of x-ray scattering cross sections for dense plasmas created by subjecting aluminum foils to strong laser-driven shocks. A narrow cone of quasimonochromatic x-rays at ~4.75 keV was used to probe the shocked part of the foil and scattered photons were detected with a CCD camera. The scattering cross section shows a clear peak, indicating diffraction from the plasma. Analysis and simulation of the data suggest that radiative heating and electron-ion energy exchange are important factors in the plasma production.

PACS numbers: 52.25.Nr, 52.35.Tc, 52.70.La

The study of dense plasmas [1,2] is of continued interest, due to their widespread occurrence in stellar objects, the interior of large planets, and inertial confinement fusion schemes. Laboratory techniques employed to diagnose such plasmas include absorption and emission spectroscopy to estimate density, temperature and ionization balance, and extended x-ray-absorption fine structure [3] to measure ion-ion correlation. A further, potentially useful technique for diagnosing ion-ion correlation is the use of x-ray scattering. The use of this technique is related to the concept of *strong coupling* [2,4], which occurs when the Coulomb energy between charged species in the plasma is greater than their thermal kinetic energy. Often this is expressed via the *strong coupling parameter*, which for ion-ion interactions is given by

$$\Gamma_{ii} = \frac{(Z^* e)^2}{R_i k T_i},$$

where $T_i$ is the ion temperature, $R_i$ is the average ion-ion separation, $k$ is Boltzmann's constant, and $Z^* e$ is the average ionic charge. If $\Gamma_{ii}$ is of order unity or greater, then there is significant short range structure in the relative arrangement of the ions. Knowledge of this would allow a structure factor for x-ray scattering to be calculated for the plasma. What this means is that we can probe the average short range structure of ions in a plasma by measuring the x-ray scattering cross section as a function of scattering angle. This is of significant interest, since the ionic correlation should have an effect on important bulk plasma properties such as thermal and electrical conductivity. Furthermore, the position and width of any peak in scattering should depend on the plasma density and temperature, thus opening the possibility of a new probe of plasma conditions against which simulations can be tested. For the plasma case, the features observed are unlikely to be as sharp as for a crystalline material. Nevertheless, diffraction-type features have been predicted for the x-ray scattering cross sections of dense plasmas [5,6] which the experiment reported here was designed to observe.

Figure 1 illustrates our experiment schematically. A target foil consisting of 3 $\mu$m of Al, coated on both sides with 1 $\mu$m of CH, was irradiated on each side by three 0.53 $\mu$m laser pulses of 550 ps FWHM duration. The beams were focused at 40° to normal with phased zone plates [7], forming a relatively flat topped 1.5 mm × 2.3 mm spot. The peak irradiance was $\sim 10^{13}$ W cm$^{-2}$. The rapid heating of the CH layer drove Mbar strength shocks, which collided in the center of the foil, compressing and heating it. The use of CH tamping allowed better uniformity in the Al layer. Combined with a moderate irradiance of $\sim 10^{13}$ W cm$^{-2}$, it also reduced the bremsstrahlung emission from the hot plasma, which would interfere with data collection. The contribution of the CH plasma to the scattering cross section is small, due to the fact that not only is

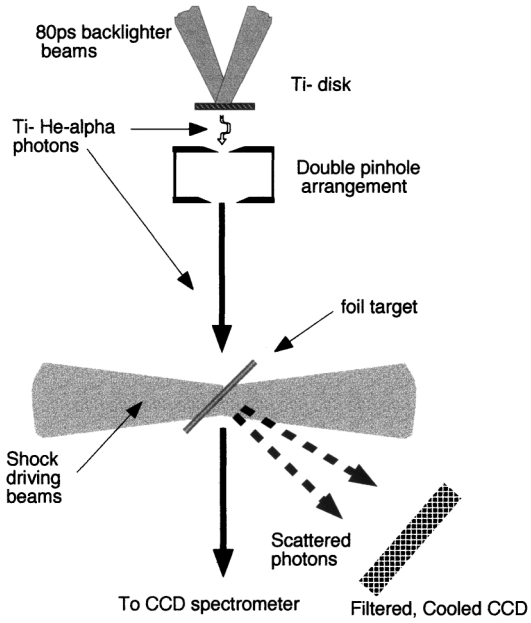


FIG. 1. Schematic of the experiment. The filters on the CCD were Mylar (50 $\mu$m), Al (25 $\mu$m), and Be (275 $\mu$m). Not shown, for clarity, is extensive shielding to prevent stray photons entering the CCD.

 0031-9007/00/84(8)/1704(4)$15.00 

the average $Z$ of the plastic lower than Al but the ions are more fully stripped and it is the scattering due to bound electrons that dominates.

Two 80 ps back-lighter beams, synchronized with the shock driving beams, were used to irradiate a 1 $\mu$m thick Ti disk. This generated an intense source of the Ti He-$\alpha$ (He-like $1s^2 1s2p\ ^1P$) and associated dielectronic satellite lines extending over 4.7–4.75 keV. The duration of emission was similar to the laser pulse duration [8]. A pair of Ta pinholes, 300 and 600 $\mu$m in diameter, restricted the photons hitting the target foil to a 5.7° cone, thus probing a 1.2 mm $\times$ 1.6 mm spot, centered on the shocked region. Most of the photons passed through the foil, down a long tube, and into a crystal spectrometer. This helped to eliminate stray He-$\alpha$ photons and also monitored probe brightness. Since the Si(111) crystal has a well known reflectivity [9] and the chip in the CCD (EEV 1511) has been calibrated [10], we can determine the flux of photons through the target. What is not shown in Fig. 1 is the extensive use of screening to prevent any photons from the back-lighter source from entering the CCD detector via any route other than scatter from the shocked foil. Null shots, to check this point, showed that such stray photons constituted typically $<3\%$ of the signal.

Since the He-$\alpha$ group is by far the brightest feature in the keV region and we filter the CCD detector against lower energy photons, we have an effectively monochromatic source for our experiment. Photons scattered from the shocked foil were detected with a 16-bit cooled x-ray CCD detector (Andor technology Instaspec IV) with 1024 $\times$ 256 pixels of 26 $\mu$m $\times$ 26 $\mu$m. This CCD subtended 18° in the horizontal plane. Since only a few hundred photons were detected per shot and each x-ray photon generated many counts (43.8 eV/count), we were able to make a histogram of the CCD to show the signal photons. The single pixel event efficiency [11] was determined for 5.9 keV photons by use of an $Fe^{55}$ source, using the "slab" model of Kraft *et al.* [12] to scale our results to 4.75 keV photons. By combining this with the known brightness of the probing beam we can determine absolute cross sections.

We have determined the cross section as a function of angle by making histograms of overlapping thirds of the CCD to achieve five data points, separated by 3°, but each being an average over 6°. Figure 2 shows cross sections for three different times relative to the peak of the shock driving beam. There are two angular positions for the CCD, one centered on 35°, the other centered at 50°. For clarity, the error bars in cross section are shown for one shot. We can see that a peak appears (~50°) only for the late time case, apparently superimposed on a broad slowly varying background which may indicate contributions from lower density, more weakly coupled plasma. At $t = +1$ ns the cross section rises with angle. At even earlier time ($t = +0.5$ ns) the cross section appears to be suppressed significantly and rises only slowly with angle. This behavior is consistent with the foil being at higher

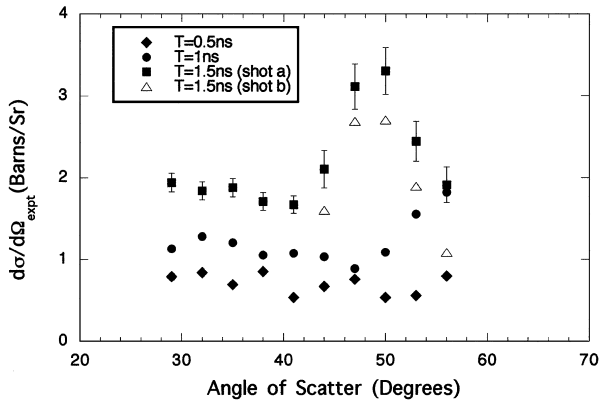


FIG. 2. Absolute scattering cross sections at various times relative to the shock driving beams. Data from 7 shots are shown, with five points per shot.

density earlier in time, as expected. It should be pointed out that for a cold foil we would expect strong features at 34°, 40°, and 66° corresponding in turn to the 111, 200, and 220 reflections for polycrystalline Al. Cold shot data, not displayed to avoid cluttering the graph, does indeed show evidence of such features. Thus, the peak at 50° is not due to cold material.

The angular distribution of the coherent part of the scattered radiation $I(q)$ is essentially governed by $I(q) \approx f(q)^2 S(q)$, where $q$ is the photon momentum change, $f(q)$ the bound electron form factor, and $S(q)$ the ion-ion structure factor. The scattering angle, for photons of wavelength $\lambda$, is derived from $q = (4\pi/\lambda)\sin(\theta/2)$. For high values of $\Gamma$, $S(q)$ should be well described by the one component plasma model (OCP). Furthermore, it has been shown [13] that in the OCP model, for $\Gamma > 40$, the peak position of the structure factor is essentially at $qa \approx 4.2$, where $a$ is the Wigner-Seitz radius. Since the bound electron form factor is expected to change very little over expected conditions, the ratio of peak scatter angles for different densities is to a good approximation

$$\frac{\sin(\theta_1/2)}{\sin(\theta_2/2)} \cong \frac{a_2}{a_1} = \frac{\rho_1^{1/3}}{\rho_2^{1/3}},$$

where $\theta_1$ and $\theta_2$ are the peak scatter angles and $a_1$ and $a_2$ are Wigner-Seitz radii corresponding to densities $\rho_1$ and $\rho_2$, respectively. By taking our experimental peak at 50 $\pm$ 3° to correspond to the OCP value of $qa = 4.2$, as described above, we can infer a mass density of 1.2 $\pm$ 0.2 g cm$^{-3}$.

The expected plasma conditions were simulated using a modified version of the one-dimensional Lagrangian hydrodynamics code MEDUSA [14]. The code treats the free electrons and ions as two separate but interacting subsystems. The energy from the laser beam and from radiation origination from hot plasma regions is absorbed by free electrons. Heating associated with shocks goes to the ions only. Energy exchange between the electrons and ions is

taken into account using the Spitzer formula for the exchange rate [2]. The radiative energy transfer is performed with a multigroup radiation transfer algorithm which uses about 100 energy groups in a choice of tabulated local thermodynamic equilibrium (LTE) opacities. A choice of equation of states including a Thomas-Fermi (TF) based [15] equation of state is also available. Figure 3 shows the predicted plasma conditions at $t = +1.5$ ns. It should be noted here that the use of various approximate opacity models (not shown) resulted in densities and temperatures which are within about 20% of the values in Fig. 3. Roughly $\frac{1}{3}$ of the target foil has a density close to 1 $\mathrm{g\,cm^{-3}}$ and a temperature of about 2 eV; the rest is hotter and at lower density. The lower density more weakly coupled component, which increases with time, may explain the rise of the broad plateau in the cross section, on which the peak sits. The simulated density of the central plasma is in good agreement with the experimentally inferred value of $1.2 \pm 0.2$ $\mathrm{g/cm^3}$. For the earlier times, the simulation predicts densities of 1.6 $\mathrm{g\,cm^{-3}}$ ($t = 1$ ns) and 3.2 $\mathrm{g\,cm^{-3}}$ ($t = 0.5$ ns). This gives expected peak angles of 55° and 72°, respectively. For the $t = 0.5$ ns case we would not expect to see the peak experimentally, as is the case. For $t = 1$ ns, we see the expected rise towards the last point at 56°. Although it is ambiguous as to whether this point represents the actual peak cross section, the data are at least consistent with the actual density being similar to the simulated value.

The angular distribution of scattered radiation for the plasma at a given density and temperature, can be calculated using the procedures in Ref. [6]. The INFERNO model [16] is used to calculate the average ionization. The ion-ion structure factors were calculated with the hypernetted-chain approximation. The calculation was calibrated by comparing the computed structure factor for liquid aluminum at 1050 °C and 2.27 $\mathrm{g\,cm^{-3}}$ with an experiment [17]. For this comparison, the Coulomb potential between the ions was assumed to be screened by the free electrons, while the best fit was obtained by assuming that the screening length was equal to $1.1a_{\mathrm{TF}}$, where $a_{\mathrm{TF}}$ is the cold Thomas-Fermi screening length. The first and second peaks of the calculated $S(q)$ nearly perfectly coincided with the liquid Al experiment [17]. These same procedures were used to generate the simulations for the plasmas in the present experiment.

The solid curve of Fig. 4 shows the results of a simulation for the predicted plasma conditions at $t = +1.5$ ns ($T_e = T_i = 2.4$ eV). The strong coupling parameter has a value of $\Gamma \sim 8$, less than the value of 40 needed for the $qa \sim$ const assumption to apply. In this case, the peak position is affected by the bound electron form factor as well as the structure factor. Although the absolute values are within a factor of 2 of the experiment, there is no satisfactory math with experiment as far as the width and position of the peak are concerned. The dashed curve corresponding to $T_i = 0.2$ eV shows a better agreement with the experiment than the one corresponding to $T_i = 2.4$ eV. We can see a much sharper peak at about the position seen experimentally. We note at this point that, without the radiative heating, MEDUSA predicts a much cooler plasma ($\sim$0.2–0.3 eV) with a higher $\Gamma$ ($\sim$100). However, the predicted densities ($>2$ $\mathrm{g\,cm^{-3}}$ for $t = 1$–1.5 ns) are significantly higher than inferred by experiment. The possibility of a low ion temperature is discussed further below.

In looking at the hydrosimulation for an explanation of the discrepancy between experiment and simulation, we looked at several issues. For the modest irradiance used, we do not expect there to be a problem with using a flux limited Spitzer heat flow. Furthermore, it was determined that by using a tabular equation of state (SESAME [18]), there was little difference in predicted plasma conditions at $t = 1.5$ ns. As we have indicated above, the use of

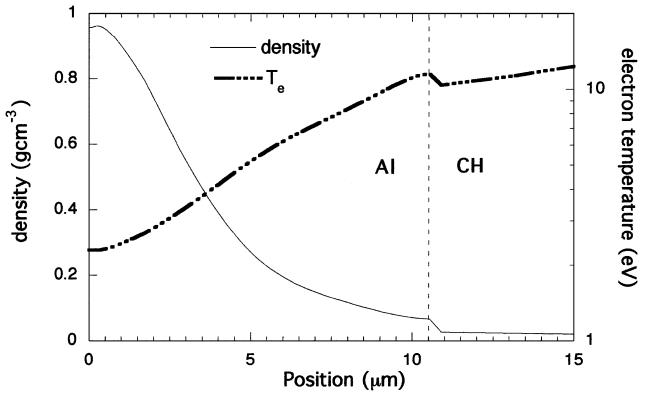


FIG. 3. Hydrodynamic simulation of target density (solid line) and electron temperature (dashed line) for a hydrodynamic simulation with radiative heating and a Thomas-Fermi based equation of state.

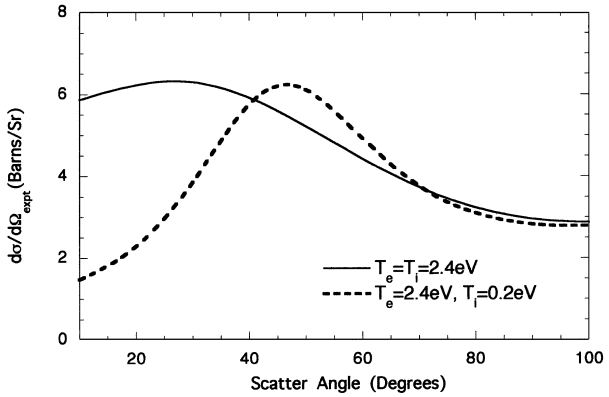


FIG. 4. Simulated x-ray scattering cross section for $t = +1.5$ ns in simulation. Both curves assume a mass density of 0.93 $\mathrm{g\,cm^{-3}}$ and an electron temperature 2.4 eV. The solid curves assume $T_i = T_e$; the dashed curve assumes $T_I = 0.2$ eV. We see that reducing the ion temperature sharpens the peak considerably.

different LTE opacity models provides values of density and temperature within approximately 20% of the values shown in Fig. 3 down to about $T_i = 1.8$ eV.

However, one way in which the value of $\Gamma$ could be higher for the predicted conditions is if the ion temperature is much lower than the electron temperature. Work by Dharma-wardana and Perrot [19] has shown that for a dense plasma the actual rate of energy exchange between electrons and ions is possibly several orders of magnitude lower than predicted by the classical equations, used in MEDUSA. Indeed, they show that for an aluminum plasma with ions at the melting temperature and an electron temperature of a few electron volts, the coupling rate is of the order of hundreds of picoseconds. Ng *et al.* [20] have explored this effect in relation to the optical emission from laser-shocked solids at comparable intensities, and they too quote energy equilibration times of order hundreds of picoseconds. In our experiment, it may be possible that the x-ray heating of the electrons provides the pressure for expansion to the experimentally inferred density, while the slow electron-ion exchange rate keeps the value of $\Gamma$ high by limiting the ion temperature. The development of an easily programmable algorithm in the hydrocode to explore this avenue is beyond the scope of our project at present. However, simulations made by simply reducing the electron-ion exchange rates by a few orders of magnitude resulted in plasma parameters which are in better agreement with those used for the dashed curve in Fig. 4. It seems that there is a potential for finding agreement between our data and simulation by exploring the issue of the electron-ion equilibration time.

In conclusion, there is wide scope for more detailed work on both the hydrodynamic simulation of this data and the methods of calculating cross sections, with the electron-ion equilibration being of particular interest. However, we can still make some significant points based on the work presented. First, we have, for the first time, measured x-ray scattering cross sections from laser-shock generated dense plasmas. Furthermore, these are absolute values and are within a factor of 2 of expectation. Second, the position of the peak has given us a relatively direct measurement of the density of the plasma at late time that is in broad agreement with hydrodynamic simulation. Finally, the lack of agreement in the width of the peak may be indicative of electron-ion relaxation times substantially longer than classical values—a point supported by other workers [19,20].

This work was supported by EPSRC Grant No. GR/K95543. We thank the staff of the Central Laser Facility without whom this work would not be possible.

*Present address: University of York, Department of Physics, Heslington, York, UK.

[1] S. Ichimaru, Rev. Mod. Phys. **51**, 1017–1057 (1982); R. M. More, in *Atoms in Unusual Situations*, edited by J. P. Briand (Plenum, New York, 1987), p. 155.
[2] R. M. More, LLNL Report No. UCRL-84991, 1981 (unpublished).
[3] T. A. Hall *et al.*, Phys. Rev. Lett. **60**, 2034 (1988).
[4] A. N. Mostovych *et al.*, Phys. Rev. Lett. **75**, 1530 (1995).
[5] E. Nardi, Phys. Rev. A **43**, 1977 (1991); J. Oliva and R. M. More, UCRL Report No. UCRL-50021-84, 1984 (unpublished).
[6] E. Nardi, Z. Zinamon, D. Riley, and N. C. Woolsey, Phys. Rev. E **57**, 4693 (1998).
[7] R. M. Stevenson *et al.*, Opt. Lett. **19**, 363 (1994).
[8] D. W. Phillion and C. J. Hailey, Phys. Rev. A **34**, 4886 (1986).
[9] B. L. Henke, E. M. Gullikson, and J. C. Davis, At. Data Nucl. Data Tables **54**, 181–342 (1993).
[10] C. Castelli *et al.*, Nucl. Instrum. Methods Phys. Res., Sect. A **310**, 240–243 (1991).
[11] K. Hashimotodani *et al.*, Rev. Sci. Instrum. **69**, 3746 (1998).
[12] R. P. Kraft *et al.*, Nucl. Instrum. Methods Phys. Res., Sect. A **366**, 192–202 (1995).
[13] S. Galam and J. P. Hansen, Phys. Rev. A **14**, 816 (1976).
[14] A. Djaoui, J. Quant. Spectrosc. Radiat. Transfer **54**, 143 (1995); J. P. Christiansen, D. E. T. F. Ashby, and K. V. Roberts, Comput. Phys. Commun. **7**, 271 (1974).
[15] A. R. Bell, Rutherford-Appleton Laboratory Report No. 80-091, 1980.
[16] D. A. Liberman, Phys. Rev. B **20**, 4981 (1979).
[17] Y. Waseda, *The Structure of Non-Crystalline Materials*, (McGraw-Hill, New York, 1980).
[18] S. P. Lyon, Los Alamos National Laboratory Report No. LAUR-923407, 1992.
[19] M. W. C. Dharma-wardana and F. Perrot, Phys. Rev. E **58**, 3705 (1998).
[20] A. Ng, P. Celliers, G. Xu, and A. Forsman, Phys. Rev. E **52**, 4299 (1995).